Check for updates

Solvothermal synthesis of Nb-doped TiO$_2$ nanoparticles with enhanced sonodynamic effects for destroying tumors†

Wenjie Sun, [ID] ‡*[a] Xiaojuan Dong,‡[b] Pingping Huang,[a] Jia Shan,[a] Lei Qi[a] and Jun Zhou [ID] *[c]

Titania (TiO$_2$) nanomaterials have been proved to be biocompatible sonosensitizers for sonodynamic therapy (SDT) of various cancer cells, while they suffer from weak sonodynamic effects due to fast combination of excited carriers. In this work, to improve the therapeutic efficiency, we prepared PEGylated Nb-doped TiO$_2$ (TiO$_{2-x}$:Nb) nanoparticles by a simple solvothermal method and a subsequent surface modification process. The TiO$_{2-x}$:Nb nanoparticles exhibited an average size of 11 nm and a polydisperse index of 0.12. The Nb doping had no obvious effect on the phase of TiO$_2$ matrixes but released electrons to the conduction band of TiO$_2$, resulting in high concentrations of deficiencies. As a result, the TiO$_{2-x}$:Nb nanoparticles exhibited a higher efficiency of singlet oxygen (^{1}O$_2$) generation than that of pure TiO$_2$ nanoparticles upon ultrasound irradiation. Importantly, the TiO$_{2-x}$:Nb nanoparticles had high biocompatibility similar to pure TiO$_2$ nanoparticles, while they could efficiently produce cytotoxic ^{1}O$_2$ to destroy cancer cells *in vitro* in comparison to the partially destroyed cancer cells by pure TiO$_2$ nanoparticles upon ultrasound irradiation. More importantly, the TiO$_{2-x}$:Nb nanoparticles displayed obvious tumor cellular injury in tumor-bearing mice *in vivo* through high SDT effects. Therefore, the synthesized PEGylated TiO$_{2-x}$:Nb nanoparticles in this study exhibited higher therapeutic effects of SDT than that of the pure TiO$_2$ nanoparticles, and the doping strategy would provide some insights for tuning traditional weak sonosensitizers into efficient ones.

Introduction

Malignant tumors with uncontrolled growth rate pose a serious threat to the suffering patients.[1,2] To treat these malignant tumors, methods including surgery, chemotherapy, and radiotherapy are commonly used, which save countless lives. However, these treatment methods still suffer from some shortcomings, for instance, the surgery is invasive and easily causes relapse, and the chemotherapy using chemical drugs causes additional side effects to the body system.[3] In order to cure or constrain the growth of malignant tumors, researchers and doctors have devoted enormous efforts to developing various kinds of new technologies such as photosensitizer-based photodynamic therapy (PDT),[4,5] near-infrared laser-driven photothermal ablation therapy (PAT),[6–9] starvation therapy,[10] and ultrasound (US)-triggered sonodynamic therapy (SDT),[11–15] which have achieved non/low invasiveness and high therapeutic efficacy for various kinds of tumors. In particular, SDT was established in the year of 1989 and utilized US to excite sonosensitizers to locally generate cytotoxic reactive oxygen species (ROS, such as singlet oxygen (^{1}O$_2$)), thus leading to irreversible oxidative damage to lipids, proteins, and/or organelles of tumor cells.[16] With the high safety and deep tissue-penetration of US, the US-triggered SDT receives increasing attention and achieves satisfactory output for malignant tumors.

The primary prerequisite for SDT is to design and synthesise sonosensitizers, which can rapidly and efficiently respond to US to produce numerous ROS. The first kind of sonosensitizers is organic molecule such as photoporphyrin and hematoporphyrin.[16] For example, Wang *et al.* prepared a functionalized nanosonosensitizer by loading sinoporphyrin sodium onto exosomes, and the nanosonosensitizers non-invasively enhanced tumor targeting and thereafter SDT toxicity.[13] However, the application of conventional organic molecules is limited by their low hydrophilicity, weak biological stability, and short blood circulation, resulting in unsatisfactory

[a]*State Key Laboratory of Ophthalmology, Optometry and Visual Science, Institute of Advanced Materials for Nano-Bio Applications, School of Ophthalmology and Optometry, School of Biomedical Engineering, Wenzhou Medical University, Wenzhou, 325035, China. E-mail: sunwj611@hotmail.com*

[b]*Center for Reproductive Medicine, Naval Medical Center of PLA, Second Military Medical University, Shanghai 200052, China*

[c]*Shanghai Xuhui Central Hospital, Zhongshan-Xuhui Hospital, Fudan University, Shanghai 200031, China. E-mail: dr_zhoujun@163.com*

† Electronic supplementary information (ESI) available. See DOI: 10.1039/d1ra06548c

‡ These authors equally contributed to this work.

therapeutic efficacy for malignant tumors. The second kind of sonosensitizers consists of inorganic sonosensitizers including hollow mesoporous silica nanoparticles (HMSNs), bimetallic oxide $MnWO_x$, and titanium oxide (TiO_2) nanoparticles.[17,18] For instance, Tachibana and co-workers reported the utilization of TiO_2 nanoparticles as sonosensitizers for the first time, and the *in vivo* results showed strong inhibition of melanoma tumors treated with TiO_2 and US.[18] It should be noted that TiO_2 nanoparticles are widely regarded as biocompatible materials, but they can only produce a few amount of ROS because of the fast electron–hole recombination within lattices. Afterwards, to improve the sensitivity of TiO_2 nanoparticles, TiO_2 nanoparticles were decorated with Au nanoparticles to form heterojunction systems or combined with two-dimensional (2D) ultrathin graphene to construct nanocomposites, thus leading to the fast separation of excited carriers.[19–21] However, the preparation process of heterojunctions or nanocomposites is complex and the resulting products are not stable, which hinders their biomedical applications. Therefore, it is still necessary to develop a new strategy to synthesize TiO_2 nanoparticles with high ROS production *via* an easy synthetic process.

Doping is an efficient strategy involving the incorporation of atoms/ions into host lattices, thus leading to unexpected properties.[22] The most well-known examples are rare-earth-based upconversion nanoparticles, which exhibit different upconversion luminescence properties by incorporating dopant ions at different species and with different amounts.[23,24] It is also well known that the TiO_2 nanomaterial can be employed as a versatile and universal matrix for doping with various ions such as hydrogen,[25,26] aluminum,[27] molybdenum,[28] and niobium (Nb).[29–34] Interestingly, the performance of TiO_2 nanomaterials could be obviously enhanced after doping, which should be ascribed to the doping-induced enhanced carrier transport within TiO_2 lattices. Among these doped nanomaterials, TiO_2 doped with Nb (TiO_2:Nb) nanomaterials exhibit tunable photoabsorption performance at different Nb-doping concentrations. For example, Chen *et al.* prepared Nb-doped TiO_2 nanocrystals through high-temperature colloidal synthesis, and the nanocrystals converted near-infrared light into thermal energy to photothermally ablate tumor cells.[35] However, the SDT effect of TiO_2:Nb nanomaterials is not well studied currently.

In the present work, we for the first time prepared PEGylated Nb-doped TiO_2 (TiO_{2-x}:Nb) nanoparticles with a narrow size distribution and high dispersibility by a simple solvothermal method and a subsequent surface modification process. After Nb doping, the Nb ions brought no obvious effect on the phase of the TiO_2 matrix but could release electrons to the conduction band of TiO_2, which resulted in high concentrations of deficiencies. Under the irradiation of US, the TiO_{2-x}:Nb nanoparticles displayed a higher $^1O_2$ generation efficiency than that of the pure TiO_2 nanoparticles. In addition, the cytotoxicity test *in vitro* proved the high biocompatibility of TiO_{2-x}:Nb nanoparticles. Under the US excitation, the TiO_{2-x}:Nb-incubated cells were efficiently destroyed in comparison to the partially destroyed TiO_2-cultured cells, showing the high killing

efficiency *in vitro*. When TiO_{2-x}:Nb nanoparticles were injected into the tumor model, the tumor cells could be destroyed through strong SDT effects. Therefore, the PEGylated TiO_{2-x}:Nb nanoparticles exhibited better therapeutic effects than those of the pure TiO_2 nanoparticles.

Experimental

Chemicals

Titanium ethoxide ($Ti(OC_2H_5)_4$, 95%), niobium chloride ($NbCl_5$, 99%), benzyl alcohol (≥99%), carboxylated polyethylene glycol (PEG–COOH, M_w = 2500), *N,N*-dimethylformamide (DMF), and 1,3-diphenylisobenzofuran (DPBF) were received from Sigma-Aldrich. RhB–PEG–COOH (M_w = 5000) was acquired from Shanghai Yanyi Biotechnology Corporation. 2′,7′-Dichloro-fluorescin diacetate (DCFH-DA), cell counting kit-8 (CCK-8), calcein-AM, propidium iodide (PI), 4,6-diamidino-2-phenylindole (DAPI), and phosphate buffer saline (PBS) were obtained from Yuanye Bio-Technology.

Synthesis and characterization of TiO_{2-x}:Nb nanoparticles

Synthesis of pure TiO_2 nanoparticles. Pure TiO_2 nanoparticles were prepared by a simple solvothermal method. Typically, 2.0 mmol of $Ti(OC_2H_5)_4$ was added into 25 mL of benzyl alcohol solution with stirring in a glove box. After 10 min, the solution was transferred to an autoclave and heated at 200 °C for 24 h. After the system cooled naturally, the solution was taken out and centrifuged (10 000 rpm, 30 min) to obtain a white precipitate. Subsequently, the white precipitate was dispersed into deionized water and centrifuged at 10 000 rpm for 30 min, and the processes were repeated three times.

Preparation of TiO_{2-x}:Nb nanoparticles. The TiO_{2-x}:Nb nanoparticles were synthesized by a similar solvothermal method. In a typically synthetic process, 2.0 mmol of $Ti(OC_2H_5)_4$ and 0.2 mmol of $NbCl_5$ were introduced into a benzyl alcohol solution (25 mL) in a glove box. After magnetic stirring for 10 min, the above solution was added into an autoclave and heated at 200 °C for 24 h. After the reaction, a blue precipitate was obtained by centrifugation and washed with deionized water as above described.

Surface modification. To improve the hydrophilicity of TiO_{2-x}:Nb nanoparticles, they (20 mg) were further mixed with deionized water containing 50 mg of PEG–COOH, followed by stirring for 24 h. The PEGylated TiO_{2-x}:Nb nanoparticles were obtained after centrifugation and washing three times with deionized water. The same surface modification process was also applied to TiO_2 nanoparticles, and PEGylated TiO_2 nanoparticles were thus obtained.

Characterization. The morphologies and sizes of TiO_2 nanoparticles and TiO_{2-x}:Nb nanoparticles were investigated using a transmission electron microscope (TEM, JEM-2100F). Fourier transform infrared reflection (FTIR) measurements were acquired from samples in KBr pellets using an IRPrestige-21 spectrometer (Shimadzu). The phases of samples were characterized using a Bruker D4 X-ray diffractometer with a Cu Kα radiation source. The electronic states of elements were

analyzed using an X-ray photoelectron spectrometer (PHI-5400). The UV-vis photoabsorption properties of DPBF were recorded using a Shimadzu UV-1900 spectrophotometer. The concentrations of samples were determined using an inductively coupled plasma atomic emission spectrometer (ICP-AES, Prodigy) *via* heating at 90 °C for 2 h.

US-responsive singlet oxygen generation

For detecting the US-triggered $^1O_2$ generation, the DPBF DMF solution (20 μL, 1.0 mg mL^{-1}) was introduced into a TiO$_{2-x}$:Nb DMF solution (2 mL, 40 ppm). The above solution was irradiated by a US probe (2.5 W cm^{-2}, 1 MHz, 50% duty cycle) for different durations (0–6 min). The absorption spectra were recorded using a UV-vis spectrophotometer. For comparison, the oxidation efficiencies of DPBF or DPBF + TiO$_2$ upon US were also recorded at 410 nm under the other identical conditions.

Cytotoxicity *in vitro*

The standard CCK-8 method was employed to evaluate the cytotoxicity of PEGylated TiO$_2$ nanoparticles and PEGylated TiO$_{2-x}$:Nb nanoparticles. The 4T1 cells (mouse breast cancer cells) were seeded into 96-well culture plates at a density of 1 × 10^4 cells per well and cultured under standard conditions. After incubation overnight, the cells were washed and incubated with a new culture medium containing TiO$_2$ or TiO$_{2-x}$:Nb (0, 10, 20, 40, 80, and 120 ppm) for another 24 h. Subsequently, cells were washed twice with a saline solution and a medium containing CCK-8 was added to each well. The absorbance was measured at 450 nm after 2 h.

Cellular internalization and $^1O_2$ detection *in vitro*

To study the cellular internalization, TiO$_{2-x}$:Nb nanoparticles were first coated with PEG–COOH and RhB–PEG–COOH, and incubated with 4T1 cells for different durations (1, 3, 6, and 8 h). After washing three times with a saline solution, cells were imaged using a digital microscope. To examine intracellular $^1O_2$, 4T1 cells were incubated with a culture medium containing nanocrystals (TiO$_2$ or TiO$_{2-x}$:Nb) at a final concentration of 40 ppm for 4 h. Then cells were washed with saline solution, followed by the co-incubation of a serum-free medium containing DCFH-DA (100 μL, 10 μM) for 1 h. Afterwards, the cells were exposed to US irradiation for 5 min (2.5 W cm^{-2}, 1.0 MHz, 50% duty cycle). Finally, the cells were stained with DAPI and imaged using a digital microscope.

SDT *in vitro*

4T1 cells were seeded into 96-well plates (1 × 10^4 cell per well) and cultured for 24 h under standard conditions. Then, the medium was removed and replaced with a fresh one containing PEGylated TiO$_2$ nanoparticles (40 ppm) or PEGylated TiO$_{2-x}$:Nb nanoparticles (40 ppm). After co-incubation for 6 h, cells were irradiated by US treatment (2.5 W cm^{-2}, 1 MHz, 50% duty cycle) for 5 min. Subsequently, cells were washed with saline solution twice, added with a medium containing CCK-8 reagent, and incubated for 2 h. The cell viability was test by

a spectrophotometric absorbance at 450 nm. In addition, cells in the parallel group were stained with calcein-AM/PI assay and then imaged by a fluorescence microscope.

SDT *in vivo*

In this study, all animal procedures and experiments were performed in accordance with the Guidelines for Care and Use of Laboratory Animals of Wenzhou Medical University and approved by the Laboratory Animal Ethics Committee of Wenzhou Medical University. BALB/c mice (male, 4 weeks, 15–20 g) were purchased from Shanghai SLAC and subcutaneously injected with 4T1 cells (5 × 10^6 cells per mouse) on the right back. BALB/c mice with a 4T1 tumor (surface size of ∼0.5 cm) were allocated into four groups (control group, saline + US group, TiO$_2$ + US group and TiO$_{2-x}$:Nb + US group) with three mice per group. The tumors of mice in saline + US group were injected with 50 μL of saline solution, while the tumors of mice in the TiO$_{2-x}$:Nb + US group were injected with the TiO$_{2-x}$:Nb saline solution (50 μL, 40 ppm). At 2 h post injection, tumor sites were treated with US irradiation (2.5 W cm^{-2}, 1 MHz, 50% duty cycle) for 10 min. After the treatments for 24 h, mice were sacrificed and tumors were taken out, fixed with formalin, embedded in paraffin, sectioned into slices and stained with H&E assay.

For long-term observation, tumor-bearing mice were divided into four groups same to the above histological examination. The tumor sizes and body weights were measured at predetermined time points, and tumor volumes were calculated according to the formula of (tumor length) × (tumor width)^2/2. At the 15th day post treatment, mice were sacrificed for harvesting tumors.

Statistical analysis

The data were expressed as the mean value ± standard deviation (SD), and any statistical comparison between two groups was analyzed using Student's two-tailed *t* test. *p < 0.05 (significant), **p < 0.01 (moderately significant), and ***p < 0.001 (highly significant).

Results and discussion

Synthesis and characterization

The pure TiO$_2$ nanoparticles were prepared by a simple solvothermal method at 200 °C for 24 h, where Ti(OC$_2$H$_5$)$_4$ was used as a Ti source and benzyl alcohol as the solvent. To improve the hydrophilicity of TiO$_2$ nanoparticles, freshly prepared nanoparticles were mixed with PEG–COOH in deionized water, and the carboxyl group could interact with nanoparticles through covalent bonds. Compared to raw nanoparticles, the PEGylated nanoparticles exhibit new peaks at 1635 and 1106 cm^{-1}, which can be respectively indexed to the carboxylate bonds from the deprotonated carboxylic acid and C–O–C stretching vibration from the PEG chain of PEG–COOH, verifying the formation of PEGylated nanoparticles (Fig. S1, ESI†). Fig. 1a illustrates the classical crystal structure of tetragonal-structured anatase TiO$_2$, in which Ti^{4+} is bonded to
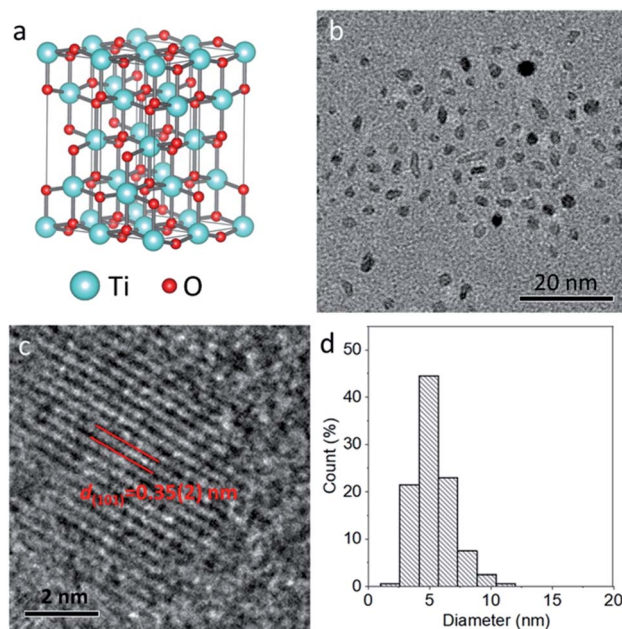
Fig. 1 (a) Crystal structure of anatase TiO_2. (b) TEM image of pure TiO_2 nanoparticles. (c) High-resolution TEM image of a TiO_2 nanoparticle showing clear lattice fringes. (d) Size histogram of pure TiO_2 nanoparticles by counting 200 nanoparticles.

Fig. 2 (a) Crystal structure of anatase TiO_{2-x}:Nb. (b) TEM image of TiO_{2-x}:Nb nanoparticles. (c) High-resolution TEM image of a TiO_{2-x}:-Nb nanoparticle. (d) Size histogram of TiO_{2-x}:Nb nanoparticles by counting 200 nanoparticles.

six equivalent O^{2-} atoms to form a mixture of corner and edge-sharing TiO_6 octahedral. Fig. 1b shows the typical TEM image of the PEGylated TiO_2 sample, in which ultrasmall nanoparticles with high uniformity and dispersibility can be observed without any aggregation. The high-resolution TEM image (Fig. 1c) reveals that a nanoparticle exhibits clear lattice fringes with an interplane d spacing of 0.35(2) nm, corresponding to the (101) plane of tetragonal-structured anatase TiO_2 (JCPDS no. 21-1272).[36] In addition, through counting 200 nanoparticles, the size histogram demonstrates the narrow size distribution of these nanoparticles, and the average size of TiO_2 nanoparticles was calculated to be 5 nm (Fig. 1d). Thus, anatase TiO_2 nanoparticles with ultrasmall and uniform size were synthesized.

Similar to the synthetic route of pure TiO_2 nanoparticles, the TiO_{2-x}:Nb nanoparticles were prepared by applying $Ti(OC_2H_5)_4$ as the Ti source, $NbCl_5$ as the Nb source, and benzyl alcohol as the solvent. With the addition of Nb element as the dopant, the color of the as-obtained TiO_{2-x}:Nb sample becomes blue in comparison to the white color for the pure TiO_2 sample (Fig. S2†). Fig. 2a shows the simulated crystal structure of TiO_{2-x}:Nb, in which Ti^{4+} ions are partly replaced by Nb^{5+} ions. For the obtained TiO_2-based nanocrystals, doping can tune their optical absorption from white TiO_2 to colored TiO_{2-x} nanocrystals (yellow, black, or blue), thus the color change for TiO_{2-x}:Nb sample suggests successful Nb doping. The TiO_{2-x}:Nb sample consists of small nanoparticles with the mainly cubic-shape, well-defined uniformity and dispersibility (Fig. 2b). The high-resolution TEM image (Fig. 2c) reveals that a nanoparticle has an interplane d spacing of 0.35(8) nm, corresponding to the (101) plane of the body-centered tetragonal-
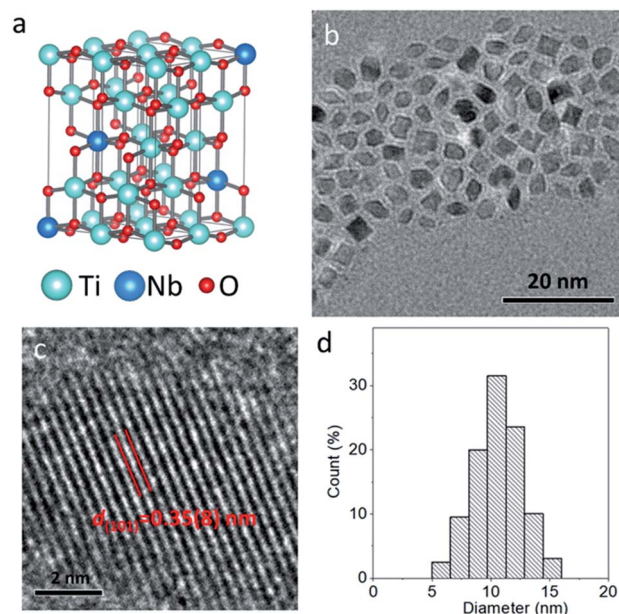
structured anatase TiO_2 (JCPDS no. 21-1272). It is worthy noted that there is no significant difference in d spacing of the (101) plane between the TiO_2 sample and the TiO_{2-x}:Nb sample, which should be ascribed to the closed ion radii as 0.605 Å for Ti^{4+} ions and 0.64 Å for Nb^{5+} ions.[35,37] As a result of Nb doping, the average size of TiO_{2-x}:Nb nanoparticles goes up to 11 nm, which is doubled compared to that (5 nm) of pure TiO_2 nanoparticles (Fig. 2d). Thus, the uniform TiO_{2-x}:Nb nanoparticles were prepared with the introduction of Nb as the dopant.

In order to study the effect of Nb doping, we performed energy-dispersive spectroscopy (EDS) and X-ray diffraction (XRD) pattern. As shown in the EDS spectrum (Fig. 3a), the pure TiO_2 sample exhibits the prominent signals of C, N, O, and Ti elements, and the Ti signal should come from TiO_2 nanoparticles. Compared to the TiO_2 sample, besides C, N, O, and Ti elements, the TiO_{2-x}:Nb sample demonstrates the additional Nb signal, which originates from the doped Nb elements (Fig. 3a and S3†). The molar ratio of Nb/(Ti + Nb) was determined to be 8.2% for the TiO_{2-x}:Nb sample. The phase of the
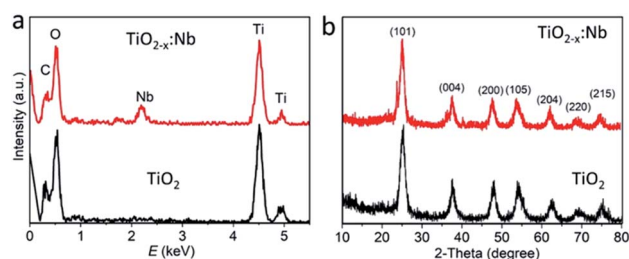

Fig. 3 (a) EDS spectra of pure TiO_2 and TiO_{2-x}:Nb nanoparticles. (b) XRD pattern of pure TiO_2 and TiO_{2-x}:Nb powder samples.

two samples was then investigated, and their XRD diffraction peaks could be well indexed to anatase TiO_2 (JCPDS no. 21-1272) without any additional peaks, indicating the high purity of samples (Fig. 3b). Specifically, the diffraction peaks of the (101), (004), (200), (105), (204), (220), and (215) planes are respectively located at 25.36°, 37.62°, 48.0°, 54.28°, 62.64°, 69.26°, and 75.32° for the pure TiO_2 sample and at 25.18°, 37.72°, 47.78°, 53.82°, 62.30°, 68.84°, and 74.72° for the TiO_{2-x}:Nb sample. Obviously, compared to the TiO_2 sample, there is a small shift of the (101) peak toward the low angle for the TiO_{2-x}:Nb sample, which should be caused by Nb doping.[37] Therefore, the above-mentioned results confirm the successful Nb doping and it brings little effect on the phase of TiO_2 matrix.

To shed more light on Ti/Nb elements within the TiO_{2-x}:Nb sample, the oxidation states were investigated by XPS analysis. The survey XPS spectrum of TiO_{2-x}:Nb nanoparticles demonstrates the strong signal of C, O, Ti, and Nb elements, as shown in Fig. S4.† The Ti 2p XPS spectrum (Fig. 4a) demonstrates the spin–orbit doublets with Ti $2p_{3/2}$ binding energy at 459.6 eV and $2p_{1/2}$ binding energy at 465.2 eV, which are in agreement with the binding energy of Ti^{4+} ions. It should be noted that there is also some asymmetry at a lower energy side for the Ti 2p spectrum, which can be fitted with Ti^{3+} states. The existence of Ti^{3+} states within TiO_{2-x}:Nb nanoparticles is due to the substitution of Nb^{5+} into Ti^{4+} sites, thus releasing electrons to the conduction band of TiO_2.[32,37] The presence of Ti^{3+} states suggests the high concentration of deficiencies within the TiO_{2-x}:Nb sample, which is similar to the previous reports. In addition, we also measured the Nb 3d XPS spectrum (Fig. 4b). The Nb 3d XPS spectrum can be well fitted into spin–orbit doublets with $3d_{5/2}$ and $3d_{3/2}$ at 207.1 and 209.9 eV, highlighting that the doped Nb is the +5 state. The O 1s XPS spectrum can also be fitted into $1s_{1/2}$ and $1s_{2/2}$, corresponding to O in the TiO_2 lattice and the ligands (Fig. S5†). Thus, we can determine the $Ti^{4+/3+}$ and Nb^{5+} ions within TiO_{2-x}:Nb nanoparticles, conferring to the high concentration of deficiencies.

$^1O_2$ generation

It has been reported that the doped TiO_2 nanoparticles exhibit the higher efficiency of US-excited $^1O_2$ generation than pure TiO_2 nanoparticles, because the doping can induce deficiencies within the lattice and, thereafter, prevent carriers from fast recombination.[38] With the Nb doping, the deficiencies can also be produced within the present TiO_{2-x}:Nb nanoparticles, which have a great potential to endow TiO_{2-x}:Nb with the elevated $^1O_2$

generation efficiency. For the detection of $^1O_2$ generated by TiO_2 nanoparticles or TiO_{2-x}:Nb nanoparticles under US irradiation, the DPBF as a probe was applied, which could be oxidized by $^1O_2$ to induce reduction of absorbance intensity. Fig. 5a shows the absorption spectra of the DPBF solution treated with TiO_{2-x}:Nb nanoparticles (40 ppm) and US (2.5 W cm^{-2}). Obviously, with the increase in irradiation time up to 6 min, the absorbance intensity goes down unceasingly, highlighting the US-triggered $^1O_2$ capacity of TiO_{2-x}:Nb nanoparticles. Moreover, we also tested the oxidation efficiency of pure TiO_2 nanoparticles (40 ppm) with US (2.5 W cm^{-2}). After US exposure for 6 min, the pure TiO_2 nanoparticles can oxidize 33.6% of DPBF, which is much lower than that (60.8%) for TiO_{2-x}:Nb nanoparticles, confirming high $^1O_2$ generation efficiency of TiO_{2-x}:Nb nanoparticles (Fig. 5b). The high efficiency should be attributed to the Nb doping-induced deficiencies within TiO_{2-x}:Nb nanoparticles, resulting in fast and efficient carrier separation, in comparison to the fast recombination of carriers within pure TiO_2 nanoparticles. In addition, there is negligible reduction in absorbance of DPBF solution upon US exposure, which suggests the US alone has no oxidization effect for DPBF. Therefore, it is concluded that the TiO_{2-x}:Nb nanoparticles exhibit higher US-triggered $^1O_2$ capacity than TiO_2 nanoparticles.

Cytocompatibility and enhanced SDT efficacy

After demonstrating the high US-triggered $^1O_2$ ability, we explored the bioapplication of TiO_{2-x}:Nb and TiO_2 nanoparticles. It has been reported that TiO_2-based nanomaterials (such as black H-TiO_2 nanoparticles and blue TiO_{2-x} nanoparticles) have been regarded as environment-friendly materials, exhibiting high biocompatibility *in vitro* and *in vivo*.[39–41] First, the cytotoxicity was evaluated by incubating 4T1 cells with the medium containing PEGylated nanoparticles at a concentration range of 0–120 ppm. After incubation for 24 h, 4T1 cells cultured with TiO_2 or TiO_{2-x}:Nb nanoparticles show the high level (>90%) of cell viability, and there is no obvious difference in cytotoxicity between TiO_2 and TiO_{2-x}:Nb nanoparticles (Fig. 6a). Thus, the cytotoxicity test proves the high biocompatibility of TiO_2 and TiO_{2-x}:Nb nanoparticles.

The cellular internalization of PEGylated nanoparticles was studied by incubating TiO_{2-x}:Nb coated with PEG–COOH and RhB–PEG–COOH for different durations (1, 3, 6, and 8 h). As
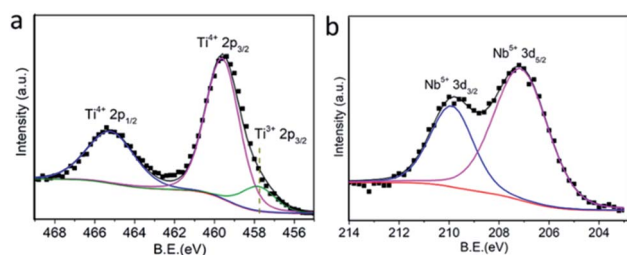

Fig. 4 (a) Ti 2p and (b) Nb 3d XPS spectrum of TiO_{2-x}:Nb samples.

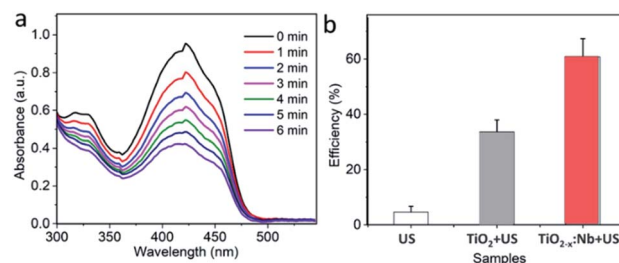**Fig. 5** (a) Absorption spectra of DPBF mediated with TiO_{2-x}:Nb nanoparticles under the irradiation of US (2.5 W cm^{-2}) over a period of 6 min. (b) Oxidation efficiency of DPBF under different conditions.

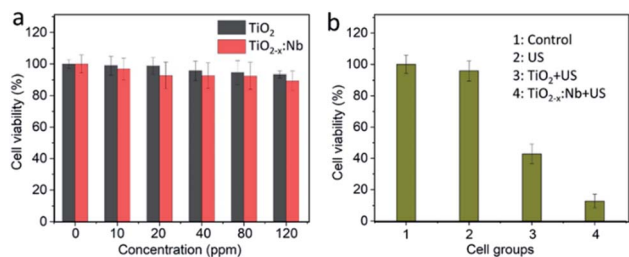**Fig. 6** (a) *In vitro* cell viability of 4T1 cells incubated with pure TiO$_2$ or TiO$_{2-x}$:Nb nanoparticles at 0–120 ppm for 24 h. (b) Cell viability of 4T1 cells incubated with TiO$_2$ (40 ppm) or TiO$_{2-x}$:Nb nanoparticles (40 ppm) and irradiated with US (2.5 W cm^{-2}, 5 min).

shown in Fig. S6,† the red fluorescence originating from RhB can be observed within cells, indicating the uptake of nanoparticles by 4T1 cells. With high biocompatibility, the SDT performance of cancer cells was investigated by first incubating 4T1 cells with PEGylated TiO$_2$ nanoparticles or TiO$_{2-x}$:Nb nanoparticles for 6 h and then exposing cells with US (2.5 W cm^{-2}, 5 min). Under the irradiation of US, cells without any treatment show high viability, which indicates the US has no SDT effect on cancer cells (Fig. 6b). With the introduction of PEGylated TiO$_2$ nanoparticles at 40 ppm, the cell viability decreases to 42.8% after US exposure. When cells were treated with the PEGylated TiO$_{2-x}$:Nb nanoparticles at the same concentration of 40 ppm and US, the viability goes down significantly to 12.8%, suggesting high killing efficiency. Furthermore, to visualize the SDT therapeutic efficiency, cells in the parallel group were treated with the same conditions and stained with calcein-AM/PI assays. As vividly shown in fluorescence images (Fig. 7), the US-irradiated cells show main green fluorescence, which is similar to cells in the control group, demonstrating the high cell activity. For cells treated with TiO$_2$ and US, the green and red fluorescence coexist, which means that only part of cells can be destroyed by the low SDT effect of pure TiO$_2$ nanoparticles. On the contrary, in the presence of TiO$_{2-x}$:Nb and US, almost all cells are killed showing strong red fluorescence. The above-mentioned results confirm that the

TiO$_{2-x}$:Nb nanoparticles have higher SDT efficiency than TiO$_2$ nanoparticles towards cancer cells *in vitro*.

Furthermore, the intracellular production of ROS was evaluated by using DCFH-DA, which could emit green fluorescence after the reaction with ^{1}O$_2$. As shown in Fig. 8 and S7,† cells treated with US or nanocrystals (TiO$_2$ or TiO$_{2-x}$:Nb) alone demonstrate extremely weak green fluorescence, which are similar to cells in the control group, indicating the low ROS level. For cells with the combination of TiO$_2$ and US, the intensity of green fluorescence within cells goes up in comparison to the control group, which indicates the production of ^{1}O$_2$ within cells. Furthermore, for cells incubated with TiO$_{2-x}$:Nb nanocrystals, there appears much stronger green fluorescence intensity than that of other groups. The strong green fluorescence confirms a large amount of ^{1}O$_2$, due to the high efficiency of US-responsiveness of TiO$_{2-x}$:Nb nanocrystals. Thus, TiO$_{2-x}$:Nb nanocrystals are capable of efficient ^{1}O$_2$ generation ability upon US irradiation, resulting in efficient cell destruction.

SDT efficacy *in vivo*

Inspired by the high biocompatibility and therapeutic efficiency *in vitro*, we further carried out SDT *in vivo*. BALB/c mice with a 4T1 tumor were randomly divided into four groups, namely, control group, saline + US group, TiO$_2$ + US group and TiO$_{2-x}$:Nb + US group. The tumors of mice in the saline + US group were injected with 50 μL of saline solution, while the tumors of mice in the TiO$_{2-x}$:Nb + US group were injected with TiO$_{2-x}$:Nb saline solution (50 μL, 40 ppm), which were illuminated with a US (2.5 W cm^{-2}) for 10 min, as illustrated in Fig. 9a. One day after treatment, mice were sacrificed, and tumors were harvested, embedded in paraffin and cryosectioned into slices. After staining with H&E assay, the tumor slices were imaged for histological examination. Fig. 9b shows the typical H&E-stained tumor slices from these groups. The slices of tumors in the control group and US group show the complete cell morphology regarding the cell size, shape and nuclear, indicating that US only has no therapeutic effect for tumors. In contrast, for the tumor slice in the TiO$_2$ + US group and the TiO$_{2-x}$:Nb + US group, cells exhibited destroyed cell membranes fused with
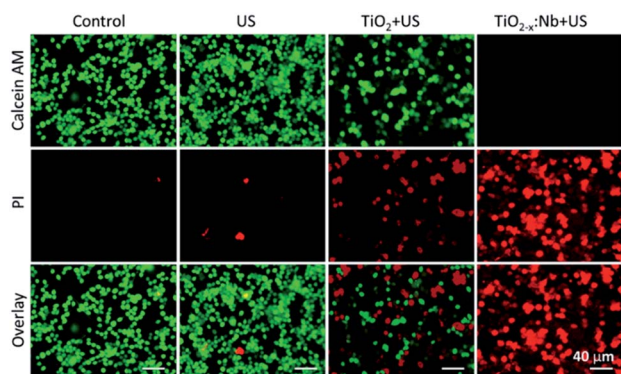

Fig. 7 Fluorescence images of calcein–AM/PI stained 4T1 cells after the treatment with PEGylated TiO$_2$ or TiO$_{2-x}$:Nb (40 ppm) and US irradiation (2.5 W cm^{-2}, 5 min).

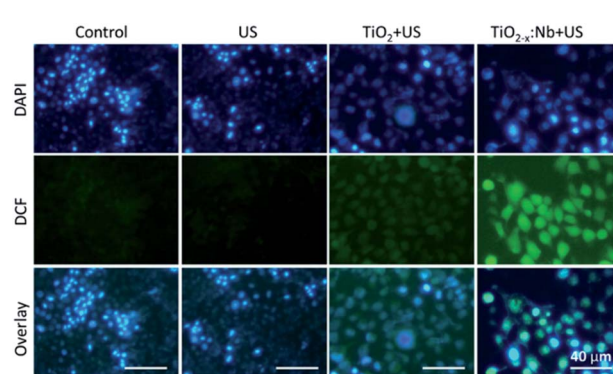**Fig. 8** Fluorescence images of DCF/DAPI-stained 4T1 cells treated with PEGylated TiO$_2$ or TiO$_{2-x}$:Nb (40 ppm) and US irradiation (2.5 W cm^{-2}, 5 min).
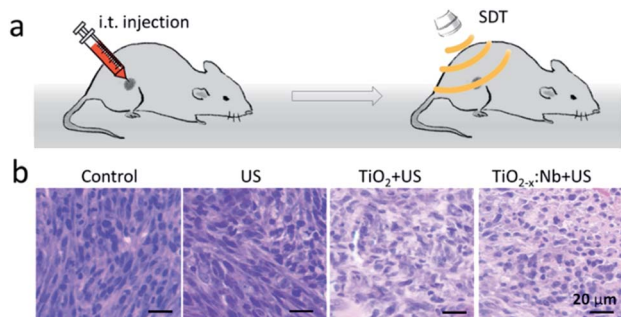
Fig. 9 (a) SDT process on tumor model by first i.t. injecting PEGylated TiO$_{2-x}$:Nb saline solution (50 μL, 40 ppm) and then exposing to US (2.5 W cm^{-2}). (b) Typical image of H&E-stained tumor slices from different groups.

intercellular substances and the condensed nucleus. Thus, the above-mentioned histological examination verifies the high SDT therapeutic effect of TiO$_{2-x}$:Nb with US exposure.

For long-term observation, tumor-bearing mice were divided into four groups similar to the above-mentioned histological examination. The growth rates of tumors in the control group and US group go up rapidly over a period of 15 days (Fig. 10a). In contrast, the tumor growth rate in the TiO$_2$ + US group is inhibited with high significance (***p < 0.001) compared with that in the control group. Moreover, the growth rate in the TiO$_{2-x}$:Nb + US group is lower than that in the TiO$_2$ + US group with **p < 0.01, due to the higher sonodynamic effect of TiO$_{2-x}$:Nb than TiO$_2$. Meanwhile, the mean weights of mice body in all groups are around 20 g (Fig. 10b). The photos of mice in Fig. 10c clearly manifest the profile of tumor growth after treatments, and there is a scar in the original tumor area in the TiO$_2$ + US group and TiO$_{2-x}$:Nb + US group. At the 15th day, mice were sacrificed for harvesting tumors, as shown in Fig. 10d. The average weights of tumors were determined to be 1.14, 1.05, 0.45, and 0.14 g in groups of control, US, TiO$_2$ + US,

and TiO$_{2-x}$:Nb + US, respectively. Therefore, TiO$_{2-x}$:Nb nanoparticles with the enhanced sonodynamic effect could achieve high tumor inhibition rates.

Conclusions

In summary, we have doped TiO$_2$ with Nb^{5+} ions for improving the sonodynamic response of TiO$_2$ for enhanced SDT of malignant tumors. The TiO$_{2-x}$:Nb nanoparticles were prepared by a new solvothermal method, where Ti(OC$_2$H$_5$)$_4$ and NbCl$_5$ in benzyl alcohol were heated in an autoclave at 200 °C for 24 h, without the strict air-free technique. The as-prepared TiO$_{2-x}$:Nb nanoparticles exhibited narrow size distribution and good dispersibility. The Nb dopants can release electrons to the conduction band, resulting in high concentrations of deficiencies within TiO$_{2-x}$:Nb. As a result of doping, the TiO$_{2-x}$:Nb nanoparticles were capable of higher US-triggered ^{1}O$_2$ generation efficiency than TiO$_2$ nanoparticles. The cytotoxicity test *in vitro* proved the high biocompatibility of TiO$_2$ and TiO$_{2-x}$:Nb nanoparticles. Under the US excitation, the TiO$_{2-x}$:Nb-incubated cells were efficiently destroyed in comparison to the partially destroyed TiO$_2$-cultured cells, showing the high killing efficiency *in vitro*. Importantly, when TiO$_{2-x}$:Nb nanoparticles were injected to the tumor model, the tumor cells can be destroyed upon US irradiation. Therefore, the PEGylated TiO$_{2-x}$:Nb nanoparticles can be served as novel nanoagents for efficient SDT.

Author contributions

W. Sun: conceptualization, methodology, resources, data curation, writing—review and editing, supervision, project administration and funding acquisition; X. Dong: methodology, writing—original draft preparation and writing—review and editing; P. Huang and J. Shan: formal analysis and writing—original draft preparation; L. Qi: resources, writing—review and editing and funding acquisition; J. Zhou: conceptualization, writing—review and editing and supervision.

Conflicts of interest

There are no conflicts to declare.

Acknowledgements

References

1 F. Bray, J. Ferlay, I. Soerjomataram, R. L. Siegel, L. A. Torre and A. Jemal, *Ca-Cancer J. Clin.*, 2018, **68**, 394–424.

2 R. L. Siegel, K. D. Miller and A. Jemal, *Ca-Cancer J. Clin.*, 2020, **70**, 7–30.

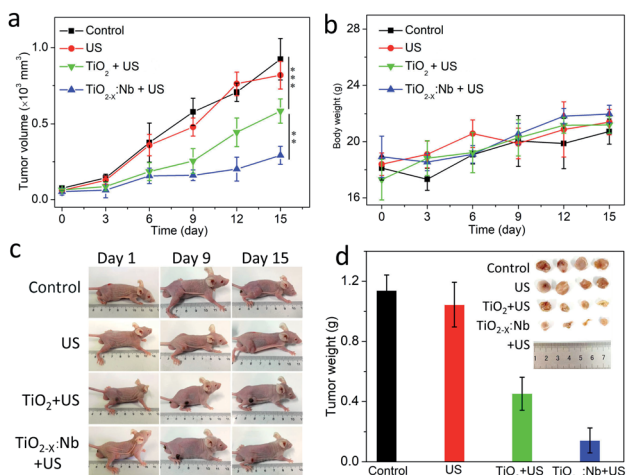3 S. Kwon, H. Ko, D. G. You, K. Kataoka and J. H. Park, *Acc. Chem. Res.*, 2019, **52**, 1771–1782.

Fig. 10 (a) Time-dependent tumor volumes after treatments. (b) Change in body weight of mice. (c) Photos of mice after treatments. (d) Photograph and the average weight of tumors.

4 W. P. Fan, P. Huang and X. Y. Chen, *Chem. Soc. Rev.*, 2016, **45**, 6488–6519.

5 L. Huang, Z. Li, Y. Zhao, Y. Zhang, S. Wu, J. Zhao and G. Han, *J. Am. Chem. Soc.*, 2016, **138**, 14586–14591.

6 B. Yang, J. Yin, Y. Chen, S. Pan, H. Yao, Y. Gao and J. Shi, *Adv. Mater.*, 2018, **30**, 1705611.

7 X. Ji, N. Kong, J. Wang, W. Li, Y. Xiao, S. T. Gan, Y. Zhang, Y. Li, X. Song, Q. Xiong, S. Shi, Z. Li, W. Tao, H. Zhang, L. Mei and J. Shi, *Adv. Mater.*, 2018, **30**, 1803031.

8 X. Yu, A. Li, C. Zhao, K. Yang, X. Chen and W. Li, *ACS Nano*, 2017, **11**, 3990–4001.

9 N. Yu, Z. Wang, J. Zhang, Z. Liu, B. Zhu, J. Yu, M. Zhu, C. Peng and Z. Chen, *Biomaterials*, 2018, **161**, 279–291.

10 Z. Lu, J. Gao, C. Fang, Y. Zhou, X. Li and G. Han, *Adv. Sci.*, 2020, **7**, 2001223.

11 X. Zheng, W. Liu, J. Ge, Q. Jia, F. Nan, Y. Ding, J. Wu, W. Zhang, C. S. Lee and P. Wang, *ACS Appl. Mater. Interfaces*, 2019, **11**, 18178–18185.

12 X. Pang, Q. Xiao, Y. Cheng, E. Ren, L. Lian, Y. Zhang, H. Gao, X. Wang, W. Leung, X. Chen, G. Liu and C. Xu, *ACS Nano*, 2019, **13**, 2427–2438.

13 Y. Liu, L. Bai, K. Guo, Y. Jia, K. Zhang, Q. Liu, P. Wang and X. Wang, *Theranostics*, 2019, **9**, 5261–5281.

14 W. Yue, L. Chen, L. Yu, B. Zhou, H. Yin, W. Ren, C. Liu, L. Guo, Y. Zhang, L. Sun, K. Zhang, H. Xu and Y. Chen, *Nat. Commun.*, 2019, **10**, 2025–2039.

15 X. Lin, Y. Qiu, L. Song, S. Chen, X. Chen, G. Huang, J. Song, X. Chen and H. Yang, *Nanoscale Horiz.*, 2019, **4**, 747–756.

16 H. Chen, X. Zhou, Y. Gao, B. Zheng, F. Tang and J. Huang, *Drug Discovery Today*, 2014, **19**, 502–509.

17 F. Gong, L. Cheng, N. Yang, O. Betzer, L. Feng, Q. Zhou, Y. Li, R. Chen, R. Popovtzer and Z. Liu, *Adv. Mater.*, 2019, **31**, 1900730.

18 Y. Harada, K. Ogawa, Y. Irie, H. Endo, L. B. Feril, T. Uemura and K. Tachibana, *J. Controlled Release*, 2011, **149**, 190–195.

19 Y. Cao, T. Wu, W. Dai, H. Dong and X. Zhang, *Chem. Mater.*, 2019, **31**, 9105–9114.

20 C. Dai, S. Zhang, Z. Liu, R. Wu and Y. Chen, *ACS Nano*, 2017, **11**, 9467–9480.

21 V. G. Deepagan, D. G. You, W. Um, H. Ko, S. Kwon, K. Y. Choi, G. R. Yi, J. Y. Lee, D. S. Lee, K. Kim, I. C. Kwon and J. H. Park, *Nano Lett.*, 2016, **16**, 6257–6264.

22 N. Yu, C. Peng, Z. Wang, Z. Liu, B. Zhu, Z. Yi, M. Zhu, X. Liu and Z. Chen, *Nanoscale*, 2018, **10**, 2542–2554.

23 F. Wang and X. Liu, *Chem. Soc. Rev.*, 2009, **38**, 976–989.

24 F. Wang, Y. Han, C. S. Lim, Y. Lu, J. Wang, J. Xu, H. Chen, C. Zhang, M. Hong and X. Liu, *Nature*, 2010, **463**, 1061–1065.

25 C. Y. Fan, C. Chen, J. Wang, X. X. Fu, Z. M. Ren, G. D. Qian and Z. Y. Wang, *Sci. Rep.*, 2015, **5**, 11712.

26 X. B. Chen, L. Liu and F. Q. Huang, *Chem. Soc. Rev.*, 2015, **44**, 1861–1885.

27 A. M. Schimpf, S. T. Ochsenbein, R. Buonsanti, D. J. Milliron and D. R. Gamelin, *Chem. Commun.*, 2012, **48**, 9352–9354.

28 K. Bhattacharyya, J. P. Majeed, K. K. Dey, P. Ayyub, A. K. Tyagi and S. R. Bharadwaj, *J. Phys. Chem. C*, 2014, 15946–15962.

29 Y. Liu, M. Liu, T. Lan, J. Dou and M. Wei, *J. Mater. Chem. A*, 2015, **3**, 18882–18888.

30 M. Kitahara, Y. Shimasaki, T. Matsuno, Y. Kuroda, A. Shimojima, H. Wada and K. Kuroda, *Chemistry*, 2015, **21**, 13073–13079.

31 X. Guo, Y. Chen, M. Su, D. Li, G. Li, C. Li, Y. Tian, C. Hao and Q. Lei, *ACS Appl. Mater. Interfaces*, 2015, **7**, 26624–26632.

32 X. J. Lu, W. G. Yang, Z. W. Quan, T. Q. Lin, L. G. Bai, L. Wang, F. Q. Huang and Y. S. Zhao, *J. Am. Chem. Soc.*, 2014, **136**, 419–426.

33 X. J. Lu, X. L. Mou, J. J. Wu, D. W. Zhang, L. L. Zhang, F. Q. Huang, F. F. Xu and S. M. Huang, *Adv. Funct. Mater.*, 2010, **20**, 509–515.

34 Y. Liu, J. M. Szeifert, J. M. Feckl, B. Mandlmeier, J. Rathousky, O. Hayden, D. Fattakhova-Rohlfing and T. Bein, *ACS Nano*, 2010, **4**, 5373–5381.

35 N. Yu, Y. Hu, X. Wang, G. Liu, Z. Wang, Z. Liu, Q. Tian, M. Zhu, X. Shi and Z. Chen, *Nanoscale*, 2017, **9**, 9148–9159.

36 T. R. Gordon, M. Cargnello, T. Paik, F. Mangolini, R. T. Weber, P. Fornasiero and C. B. Murray, *J. Am. Chem. Soc.*, 2012, **134**, 6751–6761.

37 L. D. Trizio, R. Buonsanti, A. M. Schimpf, A. Llordes, D. R. Gamelin, R. Simonutti and D. J. Milliron, *Chem. Mater.*, 2013, **25**, 3383–3390.

38 X. Han, J. Huang, X. Jing, D. Yang, H. Lin, Z. Wang, P. Li and Y. Chen, *ACS Nano*, 2018, **12**, 4545–4555.

39 W. Z. Ren, Y. Yan, L. Y. Zeng, Z. Z. Shi, A. Gong, P. Schaaf, D. Wang, J. S. Zhao, B. B. Zou, H. S. Yu, G. Chen, E. M. B. Brown and A. G. Wu, *Adv. Healthcare Mater.*, 2015, **4**, 1526–1536.

40 G. Ou, Z. Li, D. Li, L. Cheng, Z. Liu and H. Wu, *Nano Res.*, 2016, **9**, 1236–1243.

41 N. Kotagiri, G. P. Sudlow, W. J. Akers and S. Achilefu, *Nat. Nanotechnol.*, 2015, **10**, 370–379.